ChemComm

COMMUNICATION

View Article Online
View Journal | View Issue

Cite this: *Chem. Commun.*, 2019, **55**, 2485

Received 9th December 2018,
Accepted 30th January 2019

DOI: 10.1039/c8cc09747j

rsc.li/chemcomm

Hydrophilic ^{18}F-labeled *trans*-5-oxocene (oxoTCO) for efficient construction of PET agents with improved tumor-to-background ratios in neurotensin receptor (NTR) imaging†

Mengzhe Wang,‡[a] Raghu Vannam,‡[b] William D. Lambert,[b] Yixin Xie,[b] Hui Wang,[a] Benjamin Giglio,[a] Xiaofen Ma,[a] Zhanhong Wu,[a] Joseph Fox *[b] and Zibo Li *[a]

An ^{18}F-labeled *trans*-5-oxocene (oxoTCO) that is used to construct a PET probe for neurotensin receptor (NTR) imaging through tetrazine ligation is described here. PET probe construction proceeds with 70% RCY based on ^{18}F-oxoTCO and is completed within seconds. The *in vivo* behaviour of the oxoTCO based PET probe was compared with those of analogous probes that were prepared from ^{18}F-labeled s-TCO and d-TCO tracers. The hydrophilic ^{18}F-oxoTCO probe showed a significantly higher tumor-to-background ratio while displaying comparable tumor uptake relative to the ^{18}F-dTCO and ^{18}F-sTCO derived probes.

Bioorthogonal reactions are unnatural reactions that can proceed in a biological context with minimal interference from biological functionalities.[1–4] Tetrazine ligation—the inverse electron Diels–Alder reaction between s-tetrazines and alkenes—is a rapid biorthogonal reaction involving *trans*-cyclooctenes (TCOs), norbornene, cyclopropenes and α-olefins dienophiles.[5–9] The fast kinetics of the tetrazine ligation with TCO has enabled a range of biomedical applications, including applications in nuclear medicine.[10–13] We have shown that the rate of tetrazine ligation can be further accelerated through the use of conformationally strained *trans*-cyclooctene derivatives s-TCO and more hydrophilic d-TCO with rates as fast as 3.3×10^6 M^{-1} s^{-1} and 3.7×10^5 M^{-1} s^{-1}, respectively (Scheme 1A).[14,15]

Positron emission tomography (PET) is a non-invasive imaging modality that allows non-invasive monitoring of diverse biological processes *in vivo*. The most commonly used PET isotope, ^{18}F (half-life ~110 min), has become widely used for the attachment of radiolabels to biological macromolecules. In order to overcome the limitations imposed by the short half-life and the low concentration of F-18, our labs have developed fast and efficient labelling methods to generate ^{18}F-labeled PET probes with an optimized lesion-to-background contrast.[16–19] In 2010, ^{18}F-labeled TCO **1** (Scheme 1A) was described and Diels–Alder conjugates were subsequently used in a range of imaging applications.[20] More recently, we introduced ^{18}F-labeled s-TCO **2** (Scheme 1A) as the most reactive dienophile for ^{18}F probe construction, and subsequently a similar design was used by Bormans and co-workers to prepare ^{18}F-labeled s-TCO and d-TCO probes.[21–23] While the ^{18}F-attachment with these strained TCO probes is very efficient, the acquired images can have a relatively high background, leading to a modest target-to-background ratio. We hypothesized that the background is caused by the hydrophobicity of the probe, leading to a high background signal from both renal and hepatic pathways.[24]

Several approaches have been explored to improve the physiochemical properties of tetrazine ligation reaction partners. Smaller dienophiles, including cyclopropenes and cyclobutenes, have been developed as lower molecular weight alternatives to *trans*-cyclooctenes, but with a compromise of the reaction rate.[25,26] ^{18}F-labeled dialkyl-*s*-tetrazines have also been developed to increase the hydrophilicity of Diels–Alder conjugates for PET imaging applications.[27] Recently, oxygen-containing TCO derivatives with improved solubility properties have been described.[28] A *trans*-5-oxocene (oxoTCO, **4**) was shown to display enhanced reactivity compared to 5-hydroxy-*trans*-cyclooctene, and enhanced hydrophilicity ($\log P$ 0.51) relative to 5-hydroxy-*trans*-cyclooctene ($\log P$ 1.11) and d-TCO ($\log P$ 0.91). Here, we describe the preparation of labelling precursor **5** and ^{18}F-labeled oxoTCO **6**, and compare the *in vivo* imaging results for a series of probes **7b–d** that target the neurotensin (NT) receptor, which is upregulated in prostate, pancreatic, lung, and colorectal cancers.[29–32] Probes **7b–d** were prepared by combining a tetrazine–peptide conjugate **7a** with ^{18}F-s-TCO (**2**), ^{18}F-d-TCO (**3**) and ^{18}F-oxoTCO (**6**). A significant improvement in the tumor-to-background ratio was realized by using the oxoTCO-based probe **7d** in place of the more hydrophobic probes **7b** and **7c**.

Radiochemical synthesis was modeled after our previously described procedure for preparing ^{18}F-s-TCO **2**.[23] oxoTCO was

[a] *Department of Radiology and Biomedical Research Imaging Center, University of North Carolina at Chapel Hill, Chapel Hill, North Carolina 27599, USA. E-mail: ziboli@med.unc.edu*

[b] *Brown Laboratories, Department of Chemistry and Biochemistry, University of Delaware, Newark, Delaware 19716, USA. E-mail: jmfox@udel.edu*

† Electronic supplementary information (ESI) available. See DOI: 10.1039/c8cc09747j

‡ Contributed equally to the work.

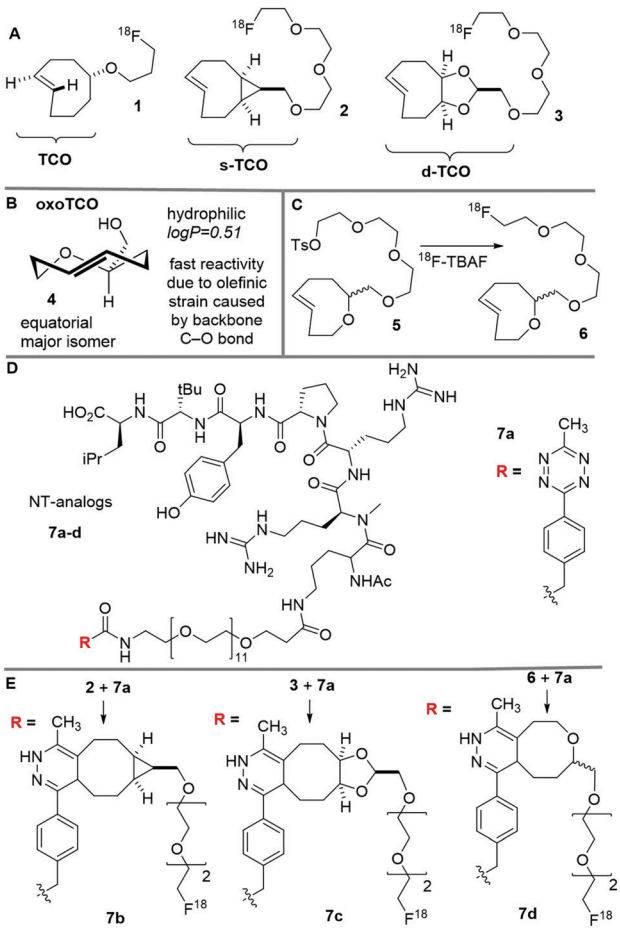

Scheme 1 (A) ^{18}F-labeled *trans*-cyclooctene radiotracers based on TCO, s-TCO and d-TCO. (B) The recently developed hetero-*trans*-cyclooctene oxoTCO displays fast reactivity and higher hydrophilicity due to the oxygen in the cyclic backbone. (C) Radio synthesis of ^{18}F-labeled oxoTCO. (D) An analog of neurotensin (NT) with a conjugated tetrazine (**7a**) is a precursor to the ^{18}F-labeled analogs for cancer imaging. (E) ^{18}F-labeled NT analogs **7b–d** from s-TCO, d-TCO, and oxoTCO, respectively. Only one isomer is shown for the Diels–Alder adducts.

prepared as a 3.4 : 1 mixture of equatorial : axial diastereomers as described previously.[28] The ^{18}F-labeling precursor **5** was prepared by treating diastereomers of oxoTCO (**4**) with triethylene glycol di(*p*-toluenesulfonate), followed by treatment with ^{18}F-TBAF to provide **6** in 15.2 ± 1.9% radiochemical yield. Efforts to improve the radiochemical yield of **6** by increasing the concentration of **5** or prolonging the reaction time were unsuccessful. While the radiochemical yield for tosylate displacement was moderate, it is high enough to be useful and is in alignment with yields obtained in many procedures for F-18 probe construction.[33] Radiolabeled s-TCO and d-TCO were prepared in a similar fashion, and cold standards were prepared using ^{19}F-TBAF. For ^{18}F-**6**, the radiochemical purity was >99% after initial purification (Fig. 1). After incubation for 1 h in PBS, the radiochemical purity of **6** was 85.2%, indicating a level of stability that was good but not as high as a cold oxoTCO compound stored under similar conditions.[28] In a previous study, we found that oxoTCO decomposes more rapidly under conditions conducive to radical formation, and it may be

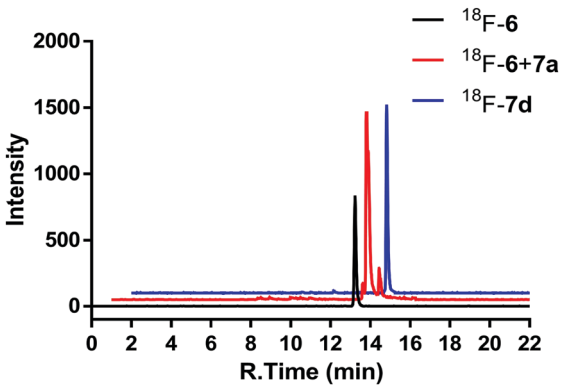

Fig. 1 Radio-HPLC profile of freshly prepared ^{18}F-**6**, crude reaction of ^{18}F-**6** and **7a** and freshly prepared ^{18}F-**7d**.

that the radiolysis contributes to the decomposition of **6**. The oxoTCO derived probe **7d** was prepared by mixing **6** with **7a**. As shown in Fig. 1, there is only one major peak which aligns with that of ^{19}F-**7d**. No ^{18}F-**6** was left indicating a complete consumption of the ^{18}F labeled oxoTCO. The reactions to prepare **7b** and **7c** were similarly efficient, and all three reactions can be completed in seconds with comparable conversion efficiency.

The log*P* values were evaluated for each of the ^{18}F-radiolabeled TCO tracers and their derived NT-probes. The log*P* value for ^{18}F-oxoTCO **6** was 0.57 ± 0.02, which was lower than those for ^{18}F-s-TCO **2** (log*P* 0.95 ± 0.02) and ^{18}F-d-TCO **3** (log*P* 0.91 ± 0.02). Similar to the corresponding dienophiles, oxoTCO-derived probe **7d** is the most hydrophilic probe with a log*P* of −2.47 ± 0.05, while s-TCO derived **7b** and d-TCO derived **7c** showed log*P* values of −1.10 ± 0.04 and −1.59 ± 0.01, respectively.

The ^{19}F-labeled NT-probe compounds were subjected to an *in vitro* competitive cell binding assay to ensure that the prosthetic linker does not compromise the binding affinity of the targeting moiety. As shown in Fig. 2, ^{19}F-labeled probes **7b–d** showed comparable binding affinity with the unmodified NT peptide. The IC_{50} values for NT, and ^{19}F-labeled probes **7b**, **7c** and **7d** are 16.2 ± 2.7 nM, 20.5 ± 14.1 nM, 15.4 ± 3.4 nM and 31.6 ± 7.1 nM, respectively.

We evaluated the *in vivo* behavior and targeting efficiency of all three PET tracers. 3.7 MBq (100 μCi) doses of **7b–d** were injected into NTR positive PC-3 tumor-bearing mice. Static

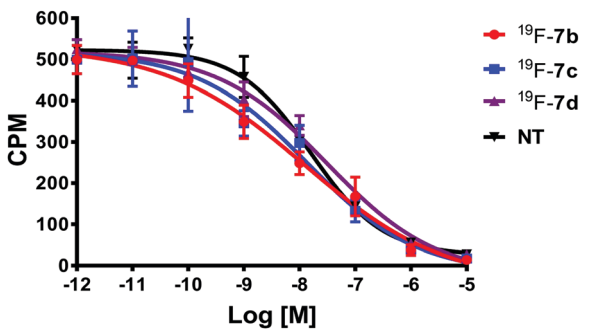

Fig. 2 Competitive cell binding assays of **7b–d** and the original NT peptide.

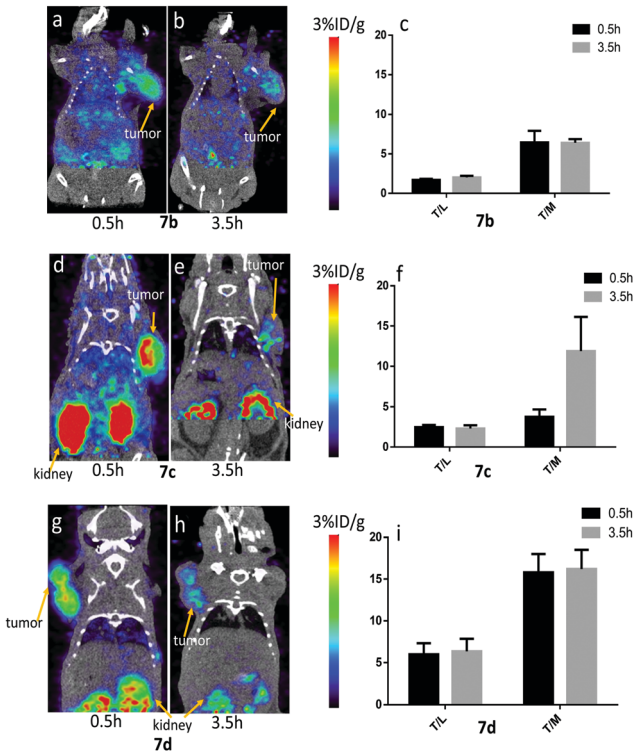

Fig. 3 Tumor-to-background ratio is improved by using oxoTCO derived **7d**. Representative PET/CT images of the PC-3 tumor-bearing mice at 0.5 h and 3.5 h post-injection with (a) and (b) **7b**, (d) and (e) **7c** and (g) and (h) **7d**. Tumor-to-liver and tumor-to-muscle ratios of (c) **7b**, (f) **7c** and (i) **7d** in the mice bearing PC-3 xenografts at 0.5 and 3.5 h post-injection.

PET/CT scans were acquired at 0.5 and 3.5 hours post injection and the images are shown in Fig. 3. As can be seen, tumors were clearly visualized in all the groups at both time points, indicating that all tracers have reasonable targeting efficiency *in vivo*. d-TCO derived tracer **7c** showed the highest tumor uptake of 2.1 ± 1.0%ID/g at 0.5 h post injection. Slightly lower uptake was observed for oxoTCO derived **7d** (1.7 ± 0.1%ID/g) and s-TCO derived **7b** (1.5 ± 0.1%ID/g). Though d-TCO derived tracer **7c** showed higher uptake than the others, there is no significant difference between any two groups. At 3.5 h post injection, the tumor uptake in all three groups decreased significantly and comparable values around 1.1%ID/g were observed.

Fig. 3 shows the representative PET/CT images of the PC-3 tumor-bearing mice after injecting probes **7b–d** and the corresponding tumor to liver and tumor to muscle ratios. Although ^{18}F-d-TCO derived **7c** showed the highest tumor uptake among the three tracers, it also showed relatively high background. High background was also observed with **7b**. The more hydrophilic ^{18}F-oxoTCO derived probe **7d** showed the highest tumor-to-liver ratio and the best tumor-to-muscle ratio among the three probes. As shown in Table 1, at 0.5 h post injection, the tumor-to-muscle ratio was 6.5 ± 1.5 and 3.8 ± 0.9 for **7b** and **7c**, while more hydrophilic **7d** showed a greatly improved tumor-to-muscle ratio of 15.8 ± 2.2. Given that the tumor uptake of **7d** is not the highest among the three compounds, it can be concluded that the high tumor-to-background ratio is due to low uptake in the muscle and the liver. At 3.5 h post injection, the high

Table 1 Tumor to muscle uptake ratio of MePhTz-NT with different TCOs in the PC-3 xenograft at 0.5 and 3.5 h post-injection

Tumor/muscle	0.5 h	3.5 h
7b	6.5 ± 1.5	6.4 ± 0.5
7c	3.8 ± 0.9	11.9 ± 4.3
7d	15.8 ± 2.2	16.2 ± 2.3

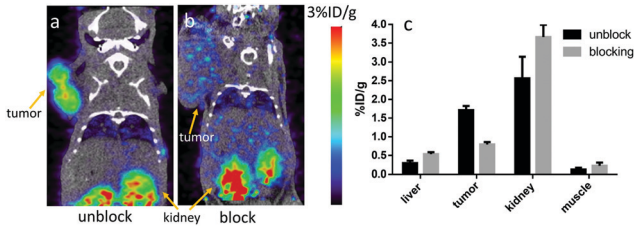

Fig. 4 Representative PET/CT images of the PC-3 tumor-bearing mice at 0.5 h post-injection of **7d** (a) without and (b) with a blocking dose. (c) Quantitative uptake of the major organs determined from the PET images.

tumor-to-muscle ratio of **7d** was maintained at 16.2 ± 2.3, indicating a faster clearance rate at non-specific binding regions than at tumor sites. The tumor to muscle ratio of **7b** remained at 6.4 ± 0.5, whereas that of **7c** increased to 11.9 ± 4.3%, an effect that is possibly related to the reduced lipophilicity of the dTCO-derived probe relative to the sTCO-derived probe. As expected, in all images, the kidneys showed the highest uptake for all PET agents, which could be attributed to the relativity small size and hydrophilicity of the three probes.

The targeting specificity of **7d** was further confirmed by a blocking experiment, in which 100 μg of NT peptide was co-injected with **7d** into PC-3 tumor-bearing mice and imaged at 0.5 h post injection (Fig. 4). The tumor uptake significantly decreased in the blocking group from 1.7 ± 0.1%ID/g to 0.8 ± 0.1%ID/g ($P < 0.05$).

In summary, an ^{18}F-labeled *trans*-5-oxocene (^{18}F-oxoTCO, **6**) for the rapid construction of PET probes *via* tetrazine ligation is described. The tracer showed comparable tumor uptake with the previously described s-TCO and d-TCO based method. However, the increased hydrophilicity of the oxoTCO enabled a faster clearance rate of the tracer from non-target organs, which led to a significantly higher tumor to background ratio compared with those of the s-TCO and d-TCO counterparts. This newly developed 18F-oxoTCO dienophile holds great potential for PET probe construction for *in vivo* applications.

This work was supported by the NIBIB (5R01EB014354-03), P30-CA016086-35-37 from the National Cancer Institute, and the UNC Radiology Department and the BRIC. Spectra were obtained using instrumentation supported by NIH grants P20GM104316, P30GM110758, S10RR026962, S10OD016267, and 1S10OD023611 and NSF grants CHE-0840401 and CHE-1229234.

Conflicts of interest

There are no conflicts to declare.

References

1 K. Lang and J. W. Chin, *ACS Chem. Biol.*, 2014, **9**, 16–20.
2 J. P. Meyer, P. Adumeau, J. S. Lewis and B. M. Zeglis, *Bioconjugate Chem.*, 2016, **27**, 2791–2807.
3 D. M. Patterson, L. A. Nazarova and J. A. Prescher, *ACS Chem. Biol.*, 2014, **9**, 592–605.
4 C. P. Ramil and Q. Lin, *Chem. Commun.*, 2013, **49**, 11007–11022.
5 M. L. Blackman, M. Royzen and J. M. Fox, *J. Am. Chem. Soc.*, 2008, **130**, 13518–13519.
6 N. K. Devaraj, R. Weissleder and S. A. Hilderbrand, *Bioconjugate Chem.*, 2008, **19**, 2297–2299.
7 Y. J. Lee, Y. Kurra, Y. Yang, J. Torres-Kolbus, A. Deiters and W. R. Liu, *Chem. Commun.*, 2014, **50**, 13085–13088.
8 A. Niederwieser, A. K. Spate, L. D. Nguyen, C. Jungst, W. Reutter and V. Wittmann, *Angew. Chem., Int. Ed.*, 2013, **52**, 4265–4268.
9 B. L. Oliveira, Z. Guo, O. Boutureira, A. Guerreiro, G. Jimenez-Oses and G. J. Bernardes, *Angew. Chem., Int. Ed. Engl.*, 2016, **55**, 14683–14687.
10 N. K. Devaraj, R. Upadhyay, J. B. Haun, S. A. Hilderbrand and R. Weissleder, *Angew. Chem., Int. Ed.*, 2009, **48**, 7013–7016.
11 T. Reiner and B. M. Zeglis, *J. Labelled Compd. Radiopharm.*, 2014, **57**, 285–290.
12 R. Rossin, T. Läppchen, S. M. van den Bosch, R. Laforest and M. S. Robillard, *J. Nucl. Med.*, 2013, **54**, 1989–1995.
13 B. M. Zeglis, K. K. Sevak, T. Reiner, P. Mohindra, S. D. Carlin, P. Zanzonico, R. Weissleder and J. S. Lewis, *J. Nucl. Med.*, 2013, **54**, 1389–1396.
14 A. Darko, S. Wallace, O. Dmitrenko, M. M. Machovina, R. A. Mehl, J. W. Chin and J. M. Fox, *Chem. Sci.*, 2014, **5**, 3770–3776.
15 M. T. Taylor, M. L. Blackman, O. Dmitrenko and J. M. Fox, *J. Am. Chem. Soc.*, 2011, **133**, 9646–9649.
16 B. C. Giglio, H. Fei, M. Wang, H. Wang, L. He, H. Feng, Z. Wu, H. Lu and Z. Li, *Theranostics*, 2017, **7**, 1524–1530.
17 Z. Wu, L. Li, S. Liu, F. Yakushijin, K. Yakushijin, D. Horne, P. S. Conti, Z. Li, F. Kandeel and J. E. Shively, *J. Nucl. Med.*, 2014, **55**, 1178–1184.
18 Z. Wu, S. Liu, M. Hassink, I. Nair, R. Park, L. Li, I. Todorov, J. M. Fox, Z. Li, J. E. Shively, P. S. Conti and F. Kandeel, *J. Nucl. Med.*, 2013, **54**, 244–251.
19 M. Wang, C. Mao, H. Wang, X. Ling, Z. Wu, Z. Li and X. Ming, *Mol. Pharmaceutics*, 2017, **14**, 3391–3398.
20 Z. Li, H. Cai, M. Hassink, M. L. Blackman, R. C. Brown, P. S. Conti and J. M. Fox, *Chem. Commun.*, 2010, **46**, 8043–8045.
21 E. M. F. Billaud, S. Belderbos, F. Cleeren, W. Maes, M. Van de Wouwer, M. Koole, A. Verbruggen, U. Himmelreich, N. Geukens and G. Bormans, *Bioconjugate Chem.*, 2017, **28**, 2915–2920.
22 E. M. F. Billaud, E. Shahbazali, M. Ahamed, F. Cleeren, T. Noel, M. Koole, A. Verbruggen, V. Hessel and G. Bormans, *Chem. Sci.*, 2017, **8**, 1251–1258.
23 M. Wang, D. Svatunek, K. Rohlfing, Y. Liu, H. Wang, B. Giglio, H. Yuan, Z. Wu, Z. Li and J. Fox, *Theranostics*, 2016, **6**, 887–895.
24 E. Kozma, I. Nikic, B. R. Varga, I. V. Aramburu, J. H. Kang, O. T. Fackler, E. A. Lemke and P. Kele, *ChemBioChem*, 2016, **17**, 1518–1524.
25 J. Yang, J. Seckute, C. M. Cole and N. K. Devaraj, *Angew. Chem., Int. Ed.*, 2012, **51**, 7476–7479.
26 K. Liu, B. Enns, B. Evans, N. Wang, X. Shang, W. Sittiwong, P. H. Dussault and J. Guo, *Chem. Commun.*, 2017, **53**, 10604–10607.
27 C. Denk, D. Svatunek, T. Filip, T. Wanek, D. Lumpi, J. Frohlich, C. Kuntner and H. Mikula, *Angew. Chem., Int. Ed.*, 2014, **53**, 9655–9659.
28 W. D. Lambert, S. L. Scinto, O. Dmitrenko, S. J. Boyd, R. Magboo, R. A. Mehl, J. W. Chin, J. M. Fox and S. Wallace, *Org. Biomol. Chem.*, 2017, **15**, 6640–6644.
29 C. Morgat, A. K. Mishra, R. Varshney, M. Allard, P. Fernandez and E. Hindie, *J. Nucl. Med.*, 2014, **55**, 1650–1657.
30 N. C. Valerie, E. V. Casarez, J. O. Dasilva, M. E. Dunlap-Brown, S. J. Parsons, G. P. Amorino and J. Dziegielewski, *Cancer Res.*, 2011, **71**, 6817–6826.
31 F. Souaze, S. Dupouy, V. Viardot-Foucault, E. Bruyneel, S. Attoub, C. Gespach, A. Gompel and P. Forgez, *Cancer Res.*, 2006, **66**, 6243–6249.
32 M. Alifano, F. Souaze, S. Dupouy, S. Camilleri-Broet, M. Younes, S. M. Ahmed-Zaid, T. Takahashi, A. Cancellieri, S. Damiani, M. Boaron, P. Broet, L. D. Miller, C. Gespach, J. F. Regnard and P. Forgez, *Clin. Cancer Res.*, 2010, **16**, 4401–4410.
33 O. Jacobson, D. O. Kiesewetter and X. Chen, *Bioconjugate Chem.*, 2015, **26**, 1–18.

